JACS
JOURNAL OF THE AMERICAN CHEMICAL SOCIETY

Communication

pubs.acs.org/JACS

Two-Dimensional $(C_4H_9NH_3)_2PbBr_4$ Perovskite Crystals for High-Performance Photodetector

Zhenjun Tan,[†,‡] Yue Wu,[†] Hao Hong,[§] Jianbo Yin,[†] Jincan Zhang,[†,‡] Li Lin,[†] Mingzhan Wang,[†] Xiao Sun,[†,‡] Luzhao Sun,[†,‡] Yucheng Huang,[†] Kaihui Liu,[§] Zhongfan Liu,*[,†] and Hailin Peng*[,†]

[†]Center for Nanochemistry, Beijing Science and Engineering Center for Nanocarbons, Beijing National Laboratory for Molecular Sciences, College of Chemistry and Molecular Engineering, Peking University, Beijing 100871, P.R. China

[‡]Academy for Advanced Interdisciplinary Studies, Peking University, Beijing 100871, P. R. China

[§]State Key Laboratory for Mesoscopic Physics, School of Physics, Peking University, Beijing 100871, P. R. China

Supporting Information

ABSTRACT: Two-dimensional (2D) layered hybrid perovskites of $(RNH_3)_2PbX_4$ (R is an alkyl and X is a halide) have been recently synthesized and exhibited rich optical properties including fluorescence and exciton effects. However, few studies on transport and optoelectronic measurements of individual 2D perovskite crystals have been reported, presumably owing to the instability issue during electronic device fabrications. Here we report the first photodetector based on individual 2D $(C_4H_9NH_3)_2PbBr_4$ perovskite crystals, built with the protection and top contact of graphene film. Both a high responsivity (~2100 A/W) and extremely low dark current (~10^{-10} A) are achieved with a design of interdigital graphene electrodes. Our study paves the way to build high-performance optoelectronic devices based on the emerging 2D single-crystal perovskite materials.

In recent years, the hybrid perovskite systems with combined advantages of organic and inorganic components, have shown remarkable potential in optoelectronic applications, such as solar cells,[1−4] light-emitting,[5] and photodetection.[6−10] The perovskite materials have a three-dimensional (3D) form or a layered two-dimensional (2D) form with a generic formula of $(RNH_3)_2(CH_3NH_3)_{m-1}A_mX_{3m+1}$, where R is an alkyl or aromatic moiety, A is a metal cation, and X is a halide.[11,12] Very recently, a new two-dimensional (2D) member of organic−inorganic hybrid perovskite family, that is, atomically thin layered crystals of $(C_4H_9NH_3)_2PbBr_4$ have been successfully synthesized by the Yang group using a solution-processed method and display high photoluminescence (PL) at room temperature.[13]

In contrast to the conventional 3D hybrid halide perovskites, the 2D layered $(C_4H_9NH_3)_2PbBr_4$ crystal consists of the inorganic layers of $[PbBr_6]^{2-}$ octahedra sandwiched between interdigitating bilayers of intercalated bulky alkylammonium cations (Figure 1a). The inorganic component offers the opportunities for high carrier mobility and a wide range of bandgap.[11−14] The organic component provides the possibility of structural diversity, highly efficient luminescence and plastic mechanical properties.[11,12] Importantly, these 2D layered perovskite crystals have a direct bandgap[15] with a high density of state (DOS) contributed by Pb orbitals, and thus exhibiting strong light−matter interaction.[15,16] In this regard, the ultrathin 2D layered perovskite crystals have shown rich optical properties, such as luminescent deep blue emission,[17] exciton effect and high absorption.[18] In addition, compared with traditional polycrystalline perovskites film, the 2D single-crystal

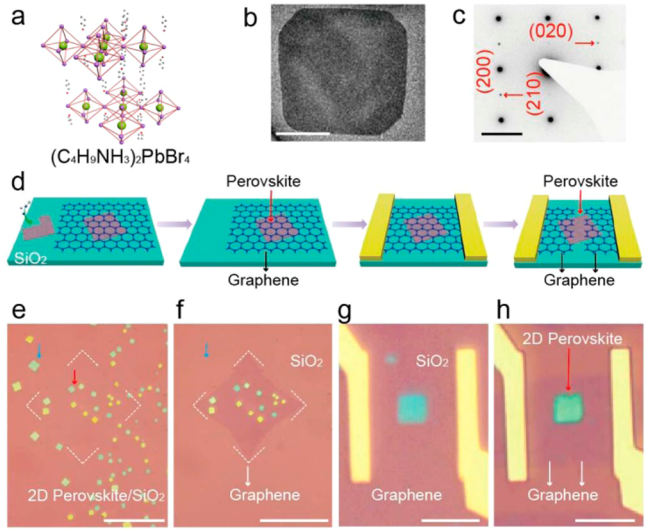

Figure 1. (a) Structural illustration of 2D layered $(C_4H_9NH_3)_2PbBr_4$ (green balls, lead atoms; mazarine blue balls, bromine atoms; small red balls, nitrogen atoms; small nattier blue balls, carbon atoms; H atoms are removed for clarity). (b) Low-magnification TEM image of a thin $(C_4H_9NH_3)_2PbBr_4$ crystal. Scale bar, 2 μm. (c) Corresponding SAED pattern with the nanosheet in panel b. Scale bar, 2 1/nm. (d) Schematics of the device fabrication process assisted with a monolayer graphene crystal. (e) Optical image (OM) of 2D $(C_4H_9NH_3)_2PbBr_4$ crystals grown on 300 nm SiO_2/silicon substrate before graphene film transfer. Scale bar, 50 μm. (f) OM image of 2D $(C_4H_9NH_3)_2PbBr_4$ crystals after dry transfer of the graphene film and dissolving in acetone. Within the white dotted line, the 2D crystals are covered by a graphene film, whereas the outside area is uncovered. Scale bar, 50 μm. (g) OM of graphene protected 2D $(C_4H_9NH_3)_2PbBr_4$ crystals before cutting out a channel. Scale bar, 10 μm. (h) Optical image for 2D $(C_4H_9NH_3)_2PbBr_4$ device with graphene electrodes. Scale bar, 10 μm.

Received: November 10, 2016
Published: December 14, 2016

DOI: 10.1021/jacs.6b11683
J. Am. Chem. Soc. 2016, 138, 16612−16615

perovskite would promise dramatically reduced defects and notably enhanced carrier diffusion length.[6,16] Consequently, the improved optical and electrical properties guarantee the potential of such new family of solution-processed semiconductors in nanoscale optoelectronic devices. However, presumably because of the instability of 2D perovskite in some solvent (e.g., acetone or water) during the microfabrication process, integration of these individual 2D perovskite crystals into specific functional nanoscale devices has still met with no success.

Here we report a facile method to build the individual 2D perovskite crystals-based photodetectors assisted with the protection and electric contact of monolayer graphene. The devices exhibit promising optoelectronic properties, such as extremely low dark current (~10^{-10} A) and high on/off current ratio (up to 10^3), which are important for high-efficiency photodetection. More importantly, through the design of graphene interdigital electrodes to enlarge the effective absorption cross section, a high photoresponsivity up to ~2100 A/W is achieved in individual 2D perovskite crystals.

2D perovskite crystals of $(C_4H_9NH_3)_2PbBr_4$ were synthesized using a solution-processed method (Details see Methods in Supporting Information (SI)).[13] Individual 2D perovskite crystals with the domain size of several to tens of micrometers can grow on arbitrary flat substrates, such as silicon dioxide, mica, fused quartz, *etc.* (Figure S1). The thicknesses of as-synthesized 2D crystals were found to be several to tens of nanometers, as determined by atomic force microscopy (AFM) (Figure S2). X-ray diffraction (XRD) and transmission electron microscopy (TEM) were conducted to examine the microstructure of as-synthesized 2D perovskite crystals. In detail, the XRD pattern reveals that the (001) planes of 2D $(C_4H_9NH_3)_2PbBr_4$ crystals grow parallel to the SiO_2 substrate, and the out-of-plane spacing (d) is about 1.42 nm (Figure S3), consistent with previously reported value.[13] As for the TEM characterization, individual 2D $(C_4H_9NH_3)_2PbBr_4$ crystals directly grow on an amorphous carbon film-coated TEM grid, showing a domain size of about 4 μm (Figure 1b). Energy-dispersive spectroscopy (EDS) was used to confirm the composition of individual 2D crystals, showing uniform elemental distribution of Pb, Br, C, and N (Figure S4). The lattice structure revealed by selected-area electron diffraction (SAED) indicated the expected lattice constants (a = 8.35 Å and b = 8.17 Å), consistent with XRD results (Figure 1c). Due to the electron radiation damage under 80 kV e-beam irradiation, only the relatively strong (200) and (020) main points and very weak (210) spots were detected, consistent with recent literature reports.[13]

For the device fabrication of individual crystals, large-area monolayer single-crystal graphene film was used as an effective cover layer for protecting these 2D perovskite crystals from the dissolution in water or acetone, without detectable degradation of the optical properties of 2D perovskite crystals (Figure 1d). To this end, sub-millimeter-sized single-crystalline graphene film was first grown on copper foil using chemical vapor deposition (CVD) method (Figure S5) and subsequently transferred onto as-synthesized 2D perovskite crystals supported by SiO_2/Si substrate with the assistance of a PMMA supporting film (Figure 2e). Note that water is carefully excluded during the transfer process by using a "dry" transfer method (Figure S6).[19] Then, the PMMA supporting layer can be removed in hot acetone, leaving entire graphene film on the 2D perovskites/substrate (Figure 2f). Interestingly, in the

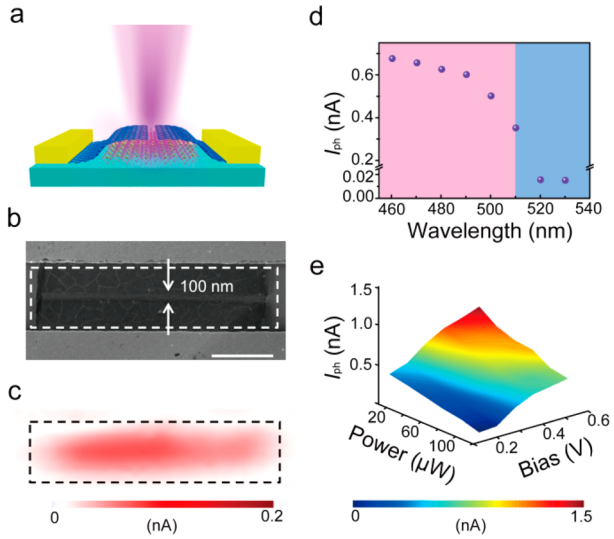

Figure 2. (a) Schematic illustration of the 2D $(C_4H_9NH_3)_2PbBr_4$ photodetector with single-crystalline graphene films acts as source-drain top electrodes. (b) SEM image of the as-fabricated device. The gap of two graphene electrodes is about 100 nm. Scale bar, 1 μm. (c) Scanning photocurrent image of the same device with a focused 470 nm incident laser. Laser spot size: 1 μm. (d) Variation of photocurrent (I_{ph}) with incident wavelength under fixed incident power. (e) 3D variation of photocurrent (I_{ph}) with incident power and bias voltage.

acetone treatment process, all of 2D perovskite crystals covered by the graphene film survived whereas the ones without graphene protection were rapidly dissolved. As shown in Figure S7, 2D perovskite crystals with the graphene coverage can survive in acetone or water for a long time, even 1 day (Figure S7). Finally, a specific processing sequence is used for building photodetectors of 2D perovskite crystals with graphene transparent electrodes. As shown in Figure 1g,h, using EBL and plasma etching,[20−22] the graphene protective layer was sacrificed gently as the source and drain electrodes with ~100 nm narrow gap. We emphasized that the 2D perovskite crystals can avoid the contact with acetone during the whole microfabrication process by using single-crystal graphene film as a protective layer and transparent source-drain electrodes, which is the key to the fabrication of high-performance optoelectronic device (Figure S8).

The photoresponse characteristics of the ultrathin $(C_4H_9NH_3)_2PbBr_4$ crystal with graphene electrodes (Figure 2a,b) were systematically investigated. First, scanning photocurrent measurements were conducted with a focused laser beam (see detailed measurement method in Supporting Information). The photocurrent mapping image (Figure 2c) demonstrates that a significant and relatively uniform photocurrent generates at the entire channel of 2D perovskite crystal. This high uniformity is presumably due to the dramatically reduced defect densities in the single crystal of perovskite. In addition, different from the vertically stacked device structure of perovskites film,[7,9,23,24] the as-fabricated lateral transport device of ultrathin 2D crystals exhibits a narrow channel (~100 nm), allowing the effective diffusion and collection of photogenerated carriers.

The photocurrent generation of ultrathin $(C_4H_9NH_3)_2PbBr_4$ crystal was investigated with different energy of incident photon (460 to 540 nm in wavelength). As shown in Figure 2d, the 2D $(C_4H_9NH_3)_2PbBr_4$ crystal exhibited a clear wavelength-dependent photoresponse: the device delivers no remarkable response

DOI: 10.1021/jacs.6b11683
J. Am. Chem. Soc. 2016, 138, 16612−16615

until the incident wavelength is below 510 nm (photon energy, 2.43 eV), which might correspond to the band gap of the 2D perovskite crystal. On the other hand, the photoresponse of our device depends on the function of incident light power and bias voltage. As shown in Figure 2e, the photocurrent increases with the increasing bias voltage and weaker incident power, revealing that the photoresponsivity can be further targetedly optimized.

For further optimizing the photoresponse, interdigital electrodes of graphene were designed to enhance the absorption cross section of 2D perovskite crystal, as presented in Figure 3a,b. In detail, the distance between each pair of

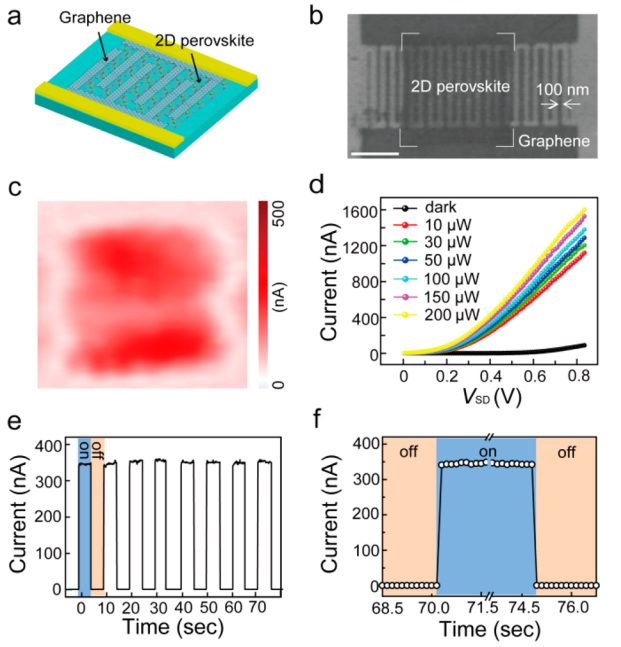

Figure 3. (a) Schematic illustration of the 2D $(C_4H_9NH_3)_2PbBr_4$ photodetector with interdigital graphene electrodes. (b) SEM image of the as-fabricated device. Scale bar, 1 μm. (c) Photocurrent mapping image recorded from the dotted area of the same device. A 470 nm laser with spot size of 1 μm focused on the device. (d) Current–voltage (I_{SD}–V_{SD}) curves of the individual device in the dark and under different illumination intensities with a 470 nm defocused laser. (e) Time-dependent photocurrent response of the device with a 470 nm defocused laser of spot size 1 mm^2, operated at a bias voltage of 0.5 V and a power of 10 μW. (f) Enlarged view of the photocurrent response during on–off illumination switching.

graphene electrodes is about 100 nm and the whole 2D perovskite crystal acts as a light sensitive material underneath graphene. Similarly, scanning photocurrent mapping (Figure 3c) was conducted to the marked area in Figure 3b, revealing that the whole area of 2D perovskite crystal displayed a uniform and enhanced photoresponse. In comparison to the perovskite photodetector with limited photosensing material (Figure 2b,c), the enlarged photosensing area and strengthened light–matter interaction promise the enhanced photocurrent generation.

To evaluate further the enhanced photoresponsivity of 2D perovskite crystal with graphene interdigital electrode, we performed photocurrent measurements of photodetectors. As illustrated in Figure 3d, the device exhibited extremely low current (10^{-10} A) in dark state, whereas under illumination the corresponding photocurrent was gradually increasing with the incident power. In contrast to the previously reported perovskites–graphene hybrid photodetector,[25,26] our 2D perovskite crystal photodetector with graphene gapped electrodes exhibits extremely low dark current, which is the key to the reliability of the perovskite photodetector. In a photoswitching measurement, the device displayed nearly 10^3 on/off current ratio even under a quite small bias (0.5 V) and weak incident power (10 μW) (Figure 3e,f). Given that the size of defocused laser spot is about 1 mm^2 and the area of whole device is about 16 μm^2, the light power received by device is calculated to be 0.16 nW. Thus, according to the definition of photoresponsivity, $R = I_{ph}/P$ (I_{ph} and P are the photocurrent and incident power, respectively), an ultrahigh photoresponsivity of 2D perovskite crystals of up to 2100 A/W was observed.

Such a reasonably efficient response in the photoconductivity experiment could be ascribed to both the strong absorption by 2D perovskite crystals and effective carrier collection by transparent graphene electrodes.[27,28] Previous measurements of similar bulk $(C_6H_5C_2H_4NH_3)_2PbI_4$ crystal indicate that the photocurrent above the band-to-band transition dominates the process at low temperature.[12,14] At room temperature, the partial ionization of the excitons into free electrons and holes would dominate and thus contribute to the enhanced photocurrent. In our case, this effect would become more prominent due to the excellent collection ability of graphene electrodes. Another appealing result in the 2D perovskite crystals-based photodetector is that the excellent on–off switching over multiple cycles shows no prominent decay, indicating the efficient encapsulation and protection of the graphene electrodes as well as the robustness of our devices.

In conclusion, we developed a facile method to overcome the instability issue of 2D perovskite crystals in solvent, and fabricated a novel photodetector composed of graphene source-drain electrodes and individual 2D $(C_4H_9NH_3)_2PbBr_4$ crystals for the first time. The intrinsic photoresponse behavior was thoroughly investigated. In the configuration of interdigital graphene electrodes, the photoconductive photodetector exhibited an ultrahigh responsivity (~2100 A/W), extremely low dark current (~10^{-10} A) and very high on/off current ratio (~10^3). Our study may open up an avenue to exploit the potential application of the 2D solution-processed perovskite crystals in optoelectronics.

■ ASSOCIATED CONTENT

Supporting Information

The Supporting Information is available free of charge on the ACS Publications website at DOI: 10.1021/jacs.6b11683.

Experimental details and supplementary figures (PDF)

■ AUTHOR INFORMATION

Corresponding Authors

*H.P. hlpeng@pku.edu.cn
*Z.L. zfliu@pku.edu.cn

ORCID

Zhongfan Liu: 0000-0003-0065-7988
Hailin Peng: 0000-0003-1569-0238

Author Contributions

Zhenjun Tan and Yue Wu contributed equally to this work.

Notes

The authors declare no competing financial interest.

DOI: 10.1021/jacs.6b11683
J. Am. Chem. Soc. 2016, 138, 16612–16615

■ ACKNOWLEDGMENTS

We acknowledge financial support from the National Basic Research Program of China (Nos. 2014CB932500, 2016YFA0200101), the National Natural Science Foundation of China (Nos. 21525310), the National Program for Support of Top-Notch Young Professionals, and Beijing Municipal Science & Technology Commission (Z161100002116002).

■ REFERENCES

(1) Kojima, A.; Teshima, K.; Shirai, Y.; Miyasaka, T. *J. Am. Chem. Soc.* **2009**, *131*, 6050.
(2) Zhou, H.; Chen, Q.; Li, G.; Luo, S.; Song, T. B.; Duan, H. S.; Hong, Z.; You, J.; Liu, Y.; Yang, Y. *Science* **2014**, *345*, 542.
(3) Burschka, J.; Pellet, N.; Moon, S. J.; Humphry-Baker, R.; Gao, P.; Nazeeruddin, M. K.; Gratzel, M. *Nature* **2013**, *499*, 316.
(4) Lee, M. M.; Teuscher, J.; Miyasaka, T.; Murakami, T. N.; Snaith, H. J. *Science* **2012**, *338*, 643.
(5) Tan, Z. K.; Moghaddam, R. S.; Lai, M. L.; Docampo, P.; Higler, R.; Deschler, F.; Price, M.; Sadhanala, A.; Pazos, L. M.; Credgington, D.; Hanusch, F.; Bein, T.; Snaith, H. J.; Friend, R. H. *Nat. Nanotechnol.* **2014**, *9*, 687.
(6) Saidaminov, M. I.; Adinolfi, V.; Comin, R.; Abdelhady, A. L.; Peng, W.; Dursun, I.; Yuan, M.; Hoogland, S.; Sargent, E. H.; Bakr, O. M. *Nat. Commun.* **2015**, *6*, 8724.
(7) Dou, L.; Yang, Y. M.; You, J.; Hong, Z.; Chang, W. H.; Li, G.; Yang, Y. *Nat. Commun.* **2014**, *5*, 5404.
(8) Wang, F.; Mei, J.; Wang, Y.; Zhang, L.; Zhao, H.; Zhao, D. *ACS Appl. Mater. Interfaces* **2016**, *8*, 2840.
(9) Deng, H.; Yang, X.; Dong, D.; Li, B.; Yang, D.; Yuan, S.; Qiao, K.; Cheng, Y. B.; Tang, J.; Song, H. *Nano Lett.* **2015**, *15*, 7963.
(10) Ramasamy, P.; Lim, D. H.; Kim, B.; Lee, S. H.; Lee, M. S.; Lee, J. S. *Chem. Commun.* **2016**, *52*, 2067.
(11) Mitzi, D. B. *J. Am. Chem. Soc.* **2001**, 1.
(12) Mitzi, D. B. In *Progress in Inorganic Chemistry*; Karlin, K. D., Ed.; John Wiley & Sons Inc: New York, NY, 1999.
(13) Dou, L.; Wong, A. B.; Yu, Y.; Lai, M.; Kornienko, N.; Eaton, S. W.; Fu, A.; Bischak, C. G.; Ma, J.; Ding, T.; Ginsberg, N. S.; Wang, L. W.; Alivisatos, A. P.; Yang, P. *Science* **2015**, *349*, 1518.
(14) Hong, X.; Ishihara, T.; Nurmikko, A. V. *Solid State Commun.* **1992**, *84*, 657.
(15) Umebayashi, T.; Asai, K.; Kondo, T.; Nakao, A. *Phys. Rev. B: Condens. Matter Mater. Phys.* **2003**, *67*, DOI: 10.1103/PhysRevB.67.155405.
(16) Brenner, T. M.; Egger, D. A.; Kronik, L.; Hodes, G.; Cahen, D. *Nat. Rev. Mater.* **2016**, *1*, 15007.
(17) Yuan, Z.; Shu, Y.; Tian, Y.; Xin, Y.; Ma, B. *Chem. Commun.* **2015**, *51*, 16385.
(18) Yaffe, O.; Chernikov, A.; Norman, Z. M.; Zhong, Y.; Velauthapillai, A.; van der Zande, A.; Owen, J. S.; Heinz, T. F. *Phys. Rev. B: Condens. Matter Mater. Phys.* **2015**, *92*, DOI: 10.1103/PhysRevB.92.045414.
(19) Wu, D.; Yan, K.; Zhou, Y.; Wang, H.; Lin, L.; Peng, H.; Liu, Z. *J. Am. Chem. Soc.* **2013**, *135*, 10926.
(20) Yin, Z. Y.; Li, H.; Li, H.; Jiang, L.; Shi, Y. M.; Sun, Y. H.; Lu, G.; Zhang, Q.; Chen, X. D.; Zhang, H. *ACS Nano* **2012**, *6*, 74.
(21) Li, H.; Yin, Z. Y.; He, Q. Y.; Li, H.; Huang, X.; Lu, G.; Fam, D. W. H.; Tok; AIY; Zhang, Q.; Zhang, H. *Small* **2012**, *8*, 63.
(22) He, Q. Y.; Wu, S. X.; Gao, S.; Cao, X. H.; Yin, Z. Y.; Li, H.; Chen, P.; Zhang, H. *ACS Nano* **2011**, *5*, 5038.
(23) Domanski, K.; Tress, W.; Moehl, T.; Saliba, M.; Nazeeruddin, M. K.; Grätzel, M. *Adv. Funct. Mater.* **2015**, *25*, 6936.
(24) Lin, Q.; Armin, A.; Lyons, D. M.; Burn, P. L.; Meredith, P. *Adv. Mater.* **2015**, *27*, 2060.
(25) Lee, Y.; Kwon, J.; Hwang, E.; Ra, C. H.; Yoo, W. J.; Ahn, J. H.; Park, J. H.; Cho, J. H. *Adv. Mater.* **2015**, *27*, 41.
(26) Wang, Y.; Zhang, Y.; Lu, Y.; Xu, W.; Mu, H.; Chen, C.; Qiao, H.; Song, J.; Li, S.; Sun, B.; Cheng, Y.-B.; Bao, Q. *Adv. Opt. Mater.* **2015**, *3*, 1389.
(27) Lee, C.-H.; Lee, G.-H.; van der Zande, A. M.; Chen, W.; Li, Y.; Han, M.; Cui, X.; Arefe, G.; Nuckolls, C.; Heinz, T. F.; Guo, J.; Hone, J.; Kim, P. *Nat. Nanotechnol.* **2014**, *9*, 676.
(28) Lin, Y.-C.; Chang, C.-Y. S.; Ghosh, R. K.; Li, J.; Zhu, H.; Addou, R.; Diaconescu, B.; Ohta, T.; Peng, X.; Lu, N.; Kim, M. J.; Robinson, J. T.; Wallace, R. M.; Mayer, T. S.; Datta, S.; Li, L.-J.; Robinson, J. A. *Nano Lett.* **2014**, *14*, 6936.

DOI: 10.1021/jacs.6b11683
J. Am. Chem. Soc. 2016, 138, 16612−16615